Heriot-Watt University
Research Gateway

Afterpulsing in Ge-on-Si Single-Photon Avalanche Diodes

Citation for published version:
Yi, X, Greener, Z, Fleming, F, Kirdoda, J, Dumas, DCS, Saalbach, L, Muir, DAS, Ferre-Llin, L, Millar, RW, Paul, DJ & Buller, GS 2023, 'Afterpulsing in Ge-on-Si Single-Photon Avalanche Diodes', *IEEE Photonics Technology Letters*, vol. 35, no. 17, pp. 959-962. https://doi.org/10.1109/LPT.2023.3289653

Digital Object Identifier (DOI):
10.1109/LPT.2023.3289653

Link:
Link to publication record in Heriot-Watt Research Portal

Document Version:
Peer reviewed version

Published In:
IEEE Photonics Technology Letters

General rights
Copyright for the publications made accessible via Heriot-Watt Research Portal is retained by the author(s) and / or other copyright owners and it is a condition of accessing these publications that users recognise and abide by the legal requirements associated with these rights.

Take down policy
Heriot-Watt University has made every reasonable effort to ensure that the content in Heriot-Watt Research Portal complies with UK legislation. If you believe that the public display of this file breaches copyright please contact open.access@hw.ac.uk providing details, and we will remove access to the work immediately and investigate your claim.

Download date: 07. Sep. 2024

Afterpulsing in Ge-on-Si Single-Photon Avalanche Diodes

Xin Yi, Zoë Greener, Fiona Fleming, Jarosław Kirdoda, Derek C. S. Dumas, Lisa Saalbach, Dave A. S. Muir, Lourdes Ferre-Llin, Ross W. Millar, Douglas J. Paul, and Gerald S. Buller

***Abstract*—In this letter, we investigate afterpulsing in 26 and 100 µm diameter planar geometry Ge-on-Si single-photon avalanche diode (SPAD) detectors, by use of the double detector gating method with a gate width of 50 ns. Ge-on-Si SPADs were found to exhibit a 1% afterpulsing probability at a delay time of 200 µs and temperature of 78 K, and 130 µs at a temperature of 150 K. These delay times were measured with an excess bias of 3.5% applied, which corresponded to a single-photon detection efficiency of 15% at 1.31 µm. We demonstrate that reducing the detector diameter can also be an effective way to restrict afterpulsing in this material system.**

***Index Terms*— Single-photon avalanche diode, Ge-on-Si, photon counting, afterpulsing, time-correlated single-photon counting, short-wave infrared.**

I. INTRODUCTION

Semiconductor based single-photon avalanche diode (SPAD) detectors are widely used in a range of applications which rely on high-resolution measurement of the arrival time of single photons, such as eye-safe light detection and ranging (LiDAR), three-dimensional imaging and sensing, quantum communication, fluorescence microscopy and many more [1]–[6]. Such detectors are also commonly known as Geiger-mode avalanche photodiodes and they are biased above the avalanche breakdown voltage. The sensitivity of such detectors is typically limited by the dark counts generated via band-to-band promotion of excited carriers through thermal excitation, trap-assisted tunneling and Shockley-Read-Hall effects. The dark count rate (DCR), however, can further increase due to the deleterious effects of afterpulsing. Here, carriers are trapped during an avalanche event and are spontaneously released at some later time, initiating further avalanche events. Afterpulsing becomes particularly problematic when a short detector dead time is required, hence minimizing this effect can be a critical in applications such as single-photon LiDAR and quantum key distribution.

Recent emerging applications that utilize light in the short-wave infrared (SWIR: 1 – 3 µm) region of the spectrum have been demonstrated using InGaAs/InP-based SPAD technology which utilizes an InGaAs absorption layer and InP multiplication layer in the separate absorption, charge and multiplication (SACM) structure [7]–[13]. There has also been research investigating SACM structures using Si and Ge for the multiplication and absorption regions, respectively [14]. One challenge is the large lattice mismatch (4.2%) between Ge and Si, which results in a high threading dislocation density, typically on the order of 10^{6}-10^{8} cm^{-2} [15]. Mesa geometry detectors have exhibited significant edge breakdown issues resulting in prohibitively high DCR and low single-photon detection efficiency (SPDE) as shown in previous studies [16]–[19]. Recently, a planar geometry Ge-on-Si SPAD with 100 µm diameter active area exhibited a noise-equivalent-power (NEP) of 7×10^{-16} $WHz^{-1/2}$ at 125 K for a wavelength of 1.31 µm [20]. Subsequently, similar geometries of Ge-on-Si SPADs with 26 µm diameter demonstrated a NEP of 9.8×10^{-17} $WHz^{-1/2}$ under similar conditions [21]. These results indicate the potential of Ge-on-Si SPADs in the SWIR region, and these detectors were used in preliminary laboratory-based LiDAR measurements [22].

In this work, afterpulsing in planar Ge-on-Si SPADs is, for the first time, systematically characterized covering a wide range of operating temperatures and excess biases above avalanche breakdown.

II. EXPERIMENTAL DETAILS

The SPAD detector is based on a separate absorption, charge and multiplication geometry, using a Ge absorption layer and a Si multiplication layer. These nominally undoped layers are separated by a p^{+} doped charge sheet in the Si, formed by selective boron ion implantation. The charge sheet controls the relative electric field of the absorber and the multiplication layers to ensure a modest electric field in the Ge layer at bias levels above avalanche breakdown. The charge sheet forms a disc, and sidewalls are etched beyond the extent of the charge sheet to electrically isolate the device as shown in Fig. 1. A more complete description of the device is given in [20] and [21]. In this paper, the charge sheet diameters considered were 26 µm and 100 µm diameter and the devices

This work was supported in part by Royal Academy of Engineering (RF-201819-18-187, CiET2021_123); Innovate UK (17706, 44835); Defence Science and Technology Laboratory (DSTLX-1000092774); Engineering and Physical Sciences Research Council (EP/N003446/1, EP/S026428/1, EPN003225/1, EP/T001011/1, EP/T00097X/1). *(Corresponding author: Xin Yi).* For the purpose of open access, the author(s) has applied a Creative Commons Attribution (CC BY) license to any Accepted Manuscript version arising.

Xin Yi, Zoë Greener, Fiona Fleming, Lisa Saalbach, Dave A. S. Muir and Gerald S. Buller are with Institute of Photonics and Quantum Sciences, School of Engineering and Physical Sciences, Heriot-Watt University, Edinburgh EH14 4AS, UK. (e-mail: xin.yi@hw.ac.uk; zmg1@hw.ac.uk; F.Fleming@hw.ac.uk; L.Saalbach@hw.ac.uk; dm140@hw.ac.uk, G.S.Buller@hw.ac.uk). Jaroslaw Kirdoda, Derek C. S. Dumas, Lourdes Ferre-Llin, Ross W. Millar and Douglas J. Paul are with James Watt School of Engineering, University of Glasgow, Rankine Building, Oakfield Avenue, Glasgow G12 8LT, U.K. (e-mail: jaroslaw.kirdoda@glasgow.ac.uk; derek.dumas@glasgow.ac.uk; Lourdes.FerreLlin@glasgow.ac.uk; Ross.Millar@glasgow.ac.uk; Douglas.Paul@glasgow.ac.uk).

were fabricated from a neighboring part of the same wafer. The avalanche breakdown voltage of the device is 41.5 V at a temperature of 175 K, reducing to 39.7 V at 78 K.

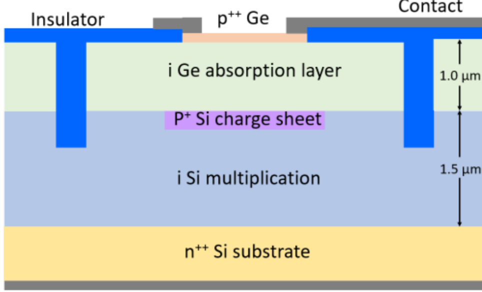

Fig. 1. Planar Ge-on-Si SPAD microstructure cross-section described in main text. The substrate is 675 µm thick.

The afterpulsing measurement setup is based on the double detector gate method [23] and multiple devices were tested. The master clock provides a trigger signal to a pulsed semiconductor diode laser at a wavelength of 1.31 µm, and to a pulse pattern generator which provides two electrical gates with a programmable delay. The first gate takes the SPAD into Geiger-mode for a pre-determined time duration in synchronization with the laser pulse, the second gate is used to measure the dark counts at a programmable delay after the first gate. The results shown in this paper are at a deliberately low laser repetition frequency of 100 Hz to allow for accurate measurement of the afterpulsing events, and the measurement time is 10 seconds for each delay time. By using a high number of incident photons in Gate 1 (typically ~200 incident photons in each gate window), we ensure that there is a near unity probability of an avalanche triggered in Gate 1, meaning that the count rate in Gate 1 exactly matches the repetition rate of that of the source. In Gate 2, we use a gate width and excess bias identical to that of Gate 1. There is no incident light present during Gate 2, so only dark events caused by both thermal excitation of carriers and afterpulsing are recorded during this period. By varying the time delay between Gate 1 and Gate 2, and measuring the dark count rate in Gate 2, it is possible to ascertain information on the afterpulsing decay of the SPAD detector. The afterpulsing probability at a pre-determined gate delay is estimated from the number of counts in Gate 2 divided by the number of counts in Gate 1.

III. Afterpulsing Results and Discussion

The afterpulsing probability versus delay time in 26 µm and 100 µm diameter Ge-on-Si SPADs measured at temperatures of 78 K is shown in Fig. 2 (a) and (b), respectively. These measurements were performed under excess biases of 1% - 4.5% of the avalanche breakdown with a gate width of 50 ns covering a wide range of delay times from 200 ns to 10 ms. We can accurately and repeatedly measure the afterpulsing probability value down to below 0.01 (i.e. 1%). Fig. 2 (a) and (b), for example, indicate that detectors operated at an excess bias of 2.5% and temperature of 78 K suffer 1% afterpulsing probability at a delay time of 100 µs for a 26 µm diameter detector, which is ×40 better than a 100 µm diameter SPAD. A smaller volume of detector not only provides a lower intrinsic background DCR as demonstrated in [21], but also reduces the afterpulsing probability. The difference in afterpulsing seen with a varying excess bias is likely due to the higher average charge flow per event as the bias is increased. Fig. 2 (c) shows that a 26 µm SPAD also has a much better afterpulsing probability compared to 100 µm when both SPADs operate at a SPDE of 20%. We also performed afterpulsing measurements under a nominally identical method and operating conditions at temperatures of 100, 125, 150, and 175 K. No data could be obtained above 175 K as the intrinsic background DCR increases and the highest excess bias the detectors can be operated at is 2.5% at 175 K.

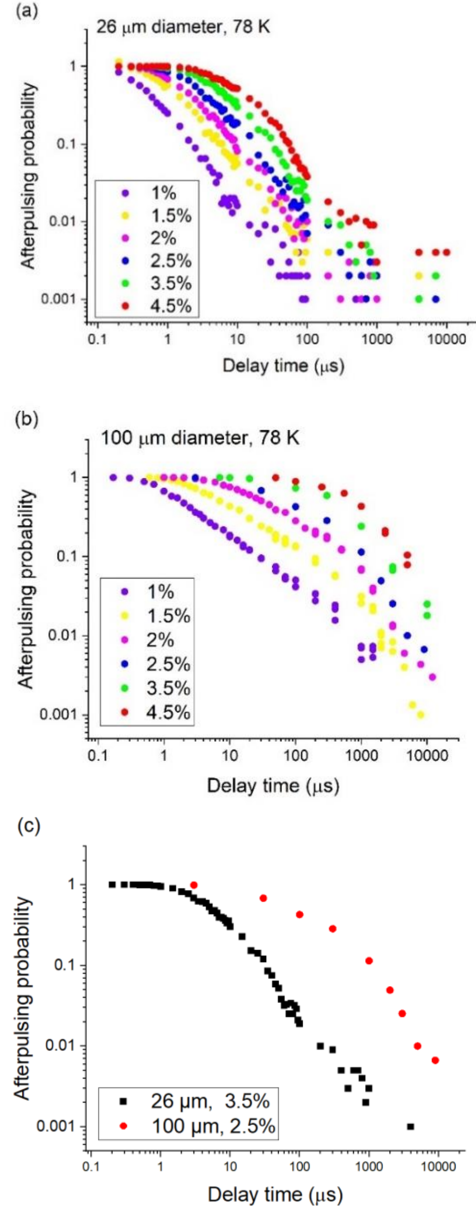

Fig. 2. (a) The afterpulsing probability as a function of the delay time in a 26 µm diameter Ge-on-Si SPAD and (b) 100 µm diameter SPAD with different excess biases on a logarithmic plot at 78 K operating temperature. (c) Afterpulsing probability comparison between 26 and 100 µm diameter SPADs at an SPDE

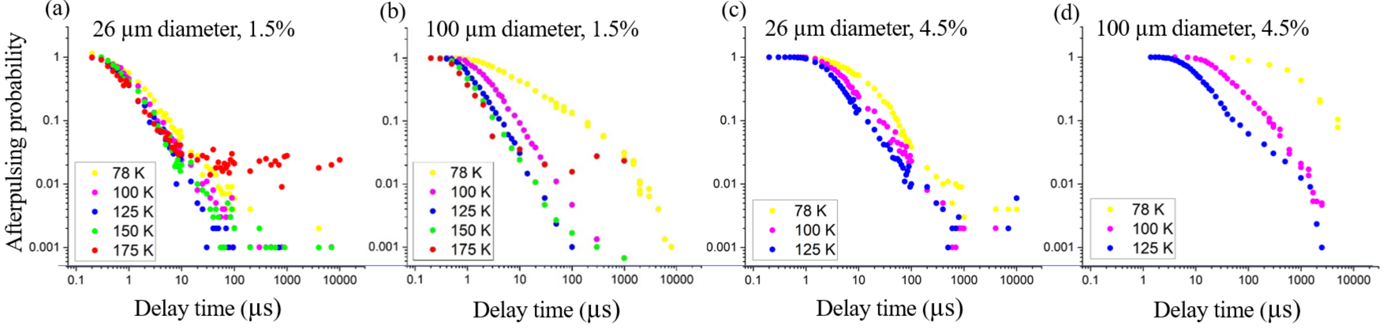

Fig. 3. Afterpulsing probability at different temperatures as a function of delay time in a (a) 26 µm and (b) 100 µm diameter SPAD respectively, at a fixed excess bias of 1.5 %. Afterpulsing probability at different temperatures in a (c) 26 µm and (d) 100 µm diameter SPAD, respectively, at a fixed excess bias of 4.5 %.

of 20% and a temperature of 78 K.

By plotting the afterpulsing probability versus delay time at an excess bias of 1.5% and 4.5% and various temperatures for a 26 and 100 µm diameter SPAD as shown in Fig. 3, it is evident that higher temperature operation reduces the afterpulsing probability in both SPADs. This temperature dependent behavior is not surprising as trapped carriers are released more rapidly at higher temperatures, as has been previously observed, for example, in InGaAs/InP SPADs [24], [25]. Fig. 3 (a) and (c) show that the temperature dependence of the afterpulsing probability in 26 µm diameter device is relatively weak. A significant afterpulsing probability is observed in the 100 µm diameter SPAD at 78 K operating temperature. However, at operating temperatures > 125 K the afterpulsing probability in the 100 µm diameter SPAD is significantly lowered and observed to be comparable to that in the 26 µm diameter SPAD. At 175 K (see red markers in Fig. 3 (a) and (b)), the intrinsic background DCR dominates the afterpulsing probability beyond a delay time of 20 µs and we do not see similar saturation at lower operating temperatures (i.e. 78 - 150 K), indicating a low intrinsic DCR at low temperatures.

We examined the characteristic decay of the afterpulsing probability found in the Ge-on-Si material by fitting an exponential model to determine the deep trapping in which the charges are confined. Using the afterpulsing probability data, the de-trapping lifetime was found by fitting the multiple exponential model given by Afterpulsing probability

$$(t) = \sum_N A_N e^{-t/\tau_N} + d \,, \qquad (1)$$

where τ_N and A_N are the de-trapping lifetime and amplitude factor for the Nth trap level and d is the intrinsic background DCR. The activation energies of carrier de-trapping were determined using the gradient of the linear fits in the Arrhenius plots (i.e. time constant versus 1/kT in eV) as shown in Fig. 4 (a) and were found to lie in the region of 7 – 30 meV for the 26 µm diameter Ge-on-Si SPADs and between 80 – 90 meV for the 100 µm diameter Ge-on-Si SPADs as shown in Fig. 4 (b). The 100 µm diameter Ge-on-Si SPAD activation energies show a low dependence on excess bias compared to those of the 26 µm Ge-on-Si SPADs which show an increase with excess bias (Fig. 4 (b) black markers). The dopants in Ge such as B and Al used for the metal contacts have activation energies of 10 meV [26], these materials are far removed from the Si avalanche region of the device and unlikely to cause any traps leading to afterpulsing. The 26 µm Ge-on-Si SPADs were fabricated with an improved GeO_2 oxidation process that demonstrated lower trap state densities than the plasma oxidation used for the 100 µm diameter devices. This thermal approach will not have oxidized the silicon at the bottom of the deep trench isolation through the Ge heterolayer in the 26 µm devices. This results in poorer native SiO_2 for those devices which could have lower electron energy trap states [27] compared to plasma oxidized SiO_2 in the 100 µm SPAD. Further work is required to identify the origins of these differences in afterpulsing behavior.

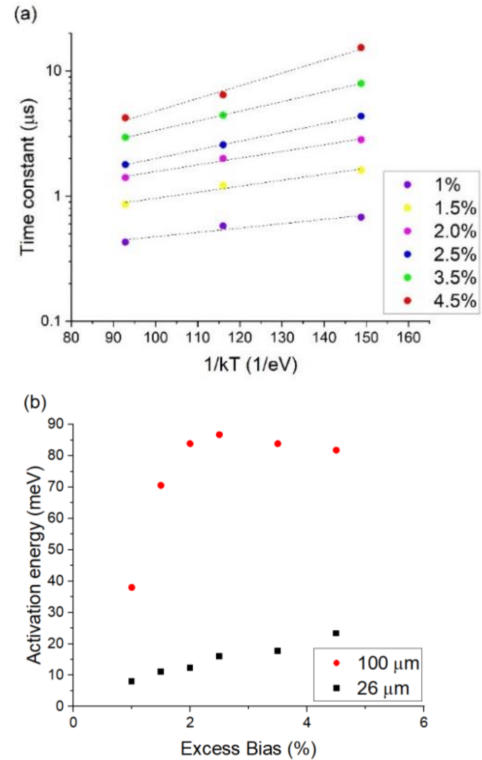

Fig. 4. (a) De-trapping lifetime for the 1st trapping level (see main text) versus 1/kT for 26 µm diameter Ge-on-Si SPADs, where k is Boltzmann's constant and T is the temperature. Black dashed lines indicate a linear fit. (b) Comparison of the

activation energy between a 26 μm and a 100 μm diameter Ge-on-Si SPAD device at various excess biases.

IV. Conclusion

The innovation of Ge-on-Si SPADs allows for the achievement of a high SPDE in the short-wave infrared region. In this letter, afterpulsing probabilities in Ge-on-Si SPADs have been experimentally investigated using the double detector gate method. The 26 μm diameter Ge-on-Si SPADs exhibited lower afterpulsing probability than the 100 μm diameter devices, which may indicate an additional trapping mechanism, possibly associated with the passivation at the bottom of the deep trench isolation closest to the avalanche region. Future generations of Ge-on-Si SPADs operating at higher temperatures compatible with Peltier cooling should be capable of operating in free-running mode or in a gated-mode where afterpulsing effects are less significant. Further studies to investigate afterpulsing in Ge-on-Si SPADs at higher operating temperatures are required to more fully explore this trend.

References

[1] A. M. Pawlikowska, A. Halimi, R. A. Lamb, and G. S. Buller, “Single-photon three-dimensional imaging at up to 10 kilometers range,” *Opt. Express*, vol. 25, no. 10, p. 11919, May 2017, doi: 10.1364/OE.25.011919.

[2] R. Tobin, A. Halimi, A. McCarthy, P. J. Soan, and G. S. Buller, “Robust real-time 3D imaging of moving scenes through atmospheric obscurant using single-photon LiDAR,” *Sci. Rep.*, vol. 11, no. 1, p. 11236, Dec. 2021, doi: 10.1038/s41598-021-90587-8.

[3] J. Tachella *et al.*, “Real-time 3D reconstruction from single-photon lidar data using plug-and-play point cloud denoisers,” *Nat. Commun.*, vol. 10, no. 1, p. 4984, Dec. 2019, doi: 10.1038/s41467-019-12943-7.

[4] R. J. Collins *et al.*, “Experimental transmission of quantum digital signatures over 90 km of installed optical fiber using a differential phase shift quantum key distribution system,” *Opt. Lett.*, vol. 41, no. 21, p. 4883, Nov. 2016, doi: 10.1364/OL.41.004883.

[5] J. Zhang, M. A. Itzler, H. Zbinden, and J.-W. Pan, “Advances in InGaAs/InP single-photon detector systems for quantum communication,” *Light Sci. Appl.*, vol. 4, no. 5, pp. e286–e286, May 2015, doi: 10.1038/lsa.2015.59.

[6] B. Korzh *et al.*, “Provably secure and practical quantum key distribution over 307 km of optical fibre,” *Nat. Photonics*, vol. 9, no. 3, pp. 163–168, Mar. 2015, doi: 10.1038/nphoton.2014.327.

[7] E. Kizilkan *et al.*, “Guard-Ring-Free InGaAs/InP Single-Photon Avalanche Diode Based on a Novel One-Step Zn-Diffusion Technique,” *IEEE J. Sel. Top. Quantum Electron.*, vol. 28, no. 5, pp. 1–9, Sep. 2022, doi: 10.1109/JSTQE.2022.3162527.

[8] F. Signorelli *et al.*, “Low-Noise InGaAs/InP Single-Photon Avalanche Diodes for Fiber-Based and Free-Space Applications,” *IEEE J. Sel. Top. Quantum Electron.*, vol. 28, no. 2, pp. 1–10, Mar. 2022, doi: 10.1109/JSTQE.2021.3104962.

[9] Y.-Q. Fang *et al.*, “InGaAs/InP single-photon detectors with 60% detection efficiency at 1550 nm,” *Rev. Sci. Instrum.*, vol. 91, no. 8, p. 083102, Aug. 2020, doi: 10.1063/5.0014123.

[10] A. Tosi, N. Calandri, M. Sanzaro, and F. Acerbi, “Low-Noise, Low-Jitter, High Detection Efficiency InGaAs/InP Single-Photon Avalanche Diode,” *IEEE J. Sel. Top. Quantum Electron.*, vol. 20, no. 6, pp. 192–197, Nov. 2014, doi: 10.1109/JSTQE.2014.2328440.

[11] S. Pellegrini *et al.*, “Design and Performance of an InGaAs–InP Single-Photon Avalanche Diode Detector,” *IEEE J. Quantum Electron.*, vol. 42, no. 4, pp. 397–403, Apr. 2006, doi: 10.1109/JQE.2006.871067.

[12] R. E. Warburton, M. Itzler, and G. S. Buller, “Free-running, room temperature operation of an InGaAs/InP single-photon avalanche diode,” *Appl. Phys. Lett.*, vol. 94, no. 7, p. 071116, Feb. 2009, doi: 10.1063/1.3079668.

[13] C. Scarcella, G. Boso, A. Ruggeri, and A. Tosi, “InGaAs/InP Single-Photon Detector Gated at 1.3 GHz With 1.5% Afterpulsing,” *IEEE J. Sel. Top. Quantum Electron.*, vol. 21, no. 3, pp. 17–22, May 2015, doi: 10.1109/JSTQE.2014.2361790.

[14] F. Thorburn *et al.*, “Ge-on-Si single-photon avalanche diode detectors for short-wave infrared wavelengths,” *J. Phys. Photonics*, vol. 4, no. 1, p. 012001, Jan. 2022, doi: 10.1088/2515-7647/ac3839.

[15] V. A. Shah, A. Dobbie, M. Myronov, and D. R. Leadley, “Reverse graded SiGe/Ge/Si buffers for high- composition virtual substrates" *J. Appl. Phys.* vol. 107, no. 6, pp. 064304, March. 2010, doi: 10.1063/1.3311556.

[16] A. Y. Loudon *et al.*, “Enhancement of the infrared detection efficiency of silicon photon-counting avalanche photodiodes by use of silicon germanium absorbing layers,” *Opt. Lett.*, vol. 27, no. 4, p. 219, Feb. 2002, doi: 10.1364/OL.27.000219.

[17] Z. Lu, Y. Kang, C. Hu, Q. Zhou, H.-D. Liu, and J. C. Campbell, “Geiger-Mode Operation of Ge-on-Si Avalanche Photodiodes,” *IEEE J. Quantum Electron.*, vol. 47, no. 5, pp. 731–735, May 2011, doi: 10.1109/JQE.2011.2110637.

[18] R. E. Warburton *et al.*, “Ge-on-Si Single-Photon Avalanche Diode Detectors: Design, Modeling, Fabrication, and Characterization at Wavelengths 1310 and 1550 nm,” *IEEE Trans. Electron Devices*, vol. 60, no. 11, pp. 3807–3813, Nov. 2013, doi: 10.1109/TED.2013.2282712.

[19] N. J. D. Martinez *et al.*, “Single photon detection in a waveguide-coupled Ge-on-Si lateral avalanche photodiode,” *Opt. Express*, vol. 25, no. 14, p. 16130, Jul. 2017, doi: 10.1364/OE.25.016130.

[20] P. Vines *et al.*, “High performance planar germanium-on-silicon single-photon avalanche diode detectors,” *Nat. Commun.*, vol. 10, no. 1, p. 1086, Dec. 2019, doi: 10.1038/s41467-019-08830-w.

[21] L. F. Llin *et al.*, “High sensitivity Ge-on-Si single-photon avalanche diode detectors,” *Opt. Lett.*, vol. 45, no. 23, p. 6406, Dec. 2020, doi: 10.1364/OL.396756.

[22] K. Kuzmenko *et al.*, “3D LIDAR imaging using Ge-on-Si single–photon avalanche diode detectors,” *Opt. Express*, vol. 28, no. 2, p. 1330, Jan. 2020, doi: 10.1364/OE.383243.

[23] S. Cova, A. Lacaita, and G. Ripamonti, “Trapping phenomena in avalanche photodiodes on nanosecond scale,” *IEEE Electron Device Lett.*, vol. 12, no. 12, pp. 685–687, Dec. 1991, doi: 10.1109/55.116955.

[24] M. Ghioni, A. Gulinatti, I. Rech, F. Zappa, and S. Cova, “Progress in Silicon Single-Photon Avalanche Diodes,” *IEEE J. Sel. Top. Quantum Electron.*, vol. 13, no. 4, pp. 852–862, 2007, doi: 10.1109/JSTQE.2007.902088.

[25] M. A. Itzler *et al.*, “Single photon avalanche diodes (SPADs) for 1.5 μm photon counting applications,” *J. Mod. Opt.*, vol. 54, no. 2–3, pp. 283–304, Jan. 2007, doi: 10.1080/09500340600792291.

[26] E. Kasper and D. J. Paul, "*Silicon Quantum Integrated Circuits*" Berlin Heidelberg: Springer-Verlag, 2005, p. 82.

[27] T. H. Nig, "High-field capture of electrons by Coulomb-attractive centers in silicon dioxide" *J. Appl. Phys.*, vol. 47, no. 7, pp. 3203 - 3208 (1976), doi: 10.1063/1.323116.